

Synthesis and Characterization of Environmentally Friendly β -Cyclodextrin Cross-Linked Cellulose/Poly(vinyl alcohol) Hydrogels for Adsorption of Malathion

Maneerat Thongrueng, Kandis Sudsakorn, Manop Charoenchaitrakool, Anusorn Seubsai, Noppadol Panchan, Sakamon Devahastin, and Chalida Niamnuy*



Cite This: *ACS Omega* 2024, 9, 22635–22649



Read Online

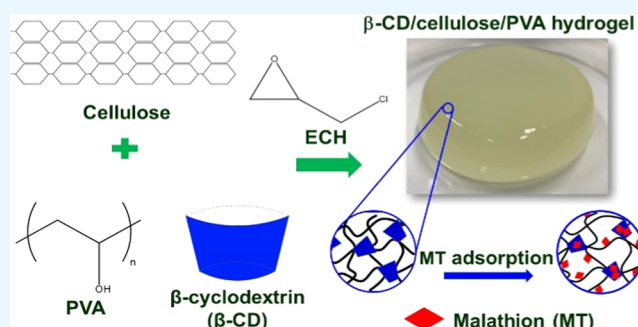
ACCESS |

Metrics & More

Article Recommendations

Supporting Information

ABSTRACT: The widespread use of malathion enhances agricultural plant productivity by eliminating pests, weeds, and diseases, but it may lead to serious environmental pollution and potential health risks for humans and animals. To mitigate these issues, environmentally friendly hydrogel adsorbents for malathion were synthesized using biodegradable polymers, specifically cellulose, β -cyclodextrin (β -CD), poly(vinyl alcohol) (PVA), and biobased epichlorohydrin as a cross-linker. This study investigated the effects of the cellulose-to-PVA ratio and epichlorohydrin (ECH) content on the properties and malathion adsorption capabilities of β -CD/cellulose/PVA hydrogels. It was found that the gel content of the hydrogels increased with a higher cellulose-to-PVA and ECH ratio, whereas the swelling ratio decreased, indicating a denser structure that impedes water permeation. In addition, various parameters affecting the malathion adsorption capacity of the hydrogel, namely, contact time, pH, hydrogel dosage, initial concentration of malathion, and temperature, were studied. The hydrogel prepared with a β -CD/cellulose/PVA ratio of 20:40:40 and 9 mL of ECH exhibited the highest malathion adsorption rate and capacity, which indicated an equilibrium adsorption capacity of 656.41 mg g⁻¹ at an initial malathion concentration of 1000 mg L⁻¹. Fourier transform infrared spectroscopy (FTIR), ζ -potential, and X-ray photoelectron spectroscopy (XPS) and NMR spectroscopy confirmed malathion adsorption within the hydrogel. The adsorption process followed intraparticle diffusion kinetics and corresponded to Freundlich isotherms, indicating multilayer adsorption on heterogeneous substrates within the adsorbent, facilitated by diffusion.



1. INTRODUCTION

Pesticides are commonly used to enhance agricultural productivity, prevent diseases, and minimize plant damage by controlling pests, worms, insects, and weeds.¹ However, the use of pesticides can lead to serious environmental issues such as ground and water contamination.² Numerous pesticides indeed exhibit hydrophobic characteristics, rendering them challenging to eliminate. Organophosphate pesticides, the most widely used class, have been applied worldwide in significant quantities annually.³ These pesticides are considered a major environmental threat and a risk to human health.⁴

Malathion (MT), an organophosphate pesticide, has been extensively used for over five decades. Human exposure to malathion can occur through various routes, such as agricultural application, consumption of treated produce, and contaminated drinking water. Malathion interferes with cholinesterase activity, leading to central nervous system disorders.⁵ Its moderate water solubility and the ineffectiveness of conventional treatment methods like sand filtration and coagulation for its removal highlight the need for more efficient techniques.⁶ Technologies such as photocatalysis, advanced

oxidation, ion exchange, and adsorption have been explored for removing malathion from water, with adsorption being preferred for its simplicity, effectiveness, safety, and cost efficiency.⁷

Different adsorbents, including activated carbons,⁸ carbon nanotubes,⁹ graphene oxides,¹⁰ metal–organic frameworks (MOFs),¹¹ resins,¹² and biosorbents,¹³ have been used to remove pesticide residues. These materials, however, often face challenges such as high costs, low efficiency, decomposition difficulties, separation issues from solutions, and sensitivity to pH levels.¹⁴ Consequently, hydrogel is an alternative adsorbent employed for the adsorption of pesticides.¹⁵ It was because their three-dimensional polymeric composites are known for

Received: January 2, 2024

Revised: May 2, 2024

Accepted: May 8, 2024

Published: May 16, 2024



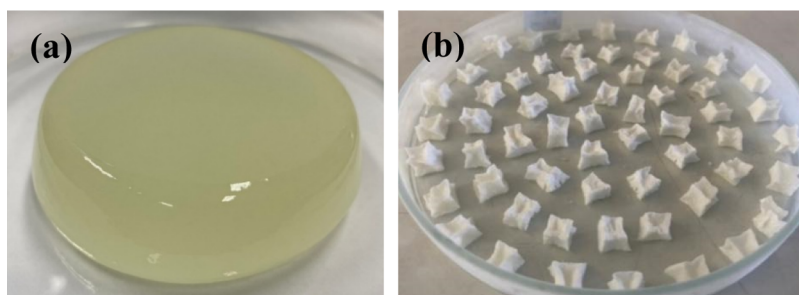


Figure 1. Photographs of β -CD/cellulose/PVA hydrogels (a) after curing and (b) after freeze-drying.

Table 1. Properties of the β -CD/Cellulose/PVA Hydrogels^a

sample	β -CD/cellulose/PVA ratio (%)	ECH content (Tomlin)	moisture content (%)	gel content (%)	swelling ratio (%)	density (g/mL)
CP1C	20:40:40	9	34.56 \pm 2.67 ^a	26.39 \pm 0.81 ^e	334.54 \pm 1.51 ^b	1.36
CP2C	20:50:30	9	34.09 \pm 3.11 ^a	27.89 \pm 0.60 ^{de}	325.73 \pm 3.23 ^c	1.39
CP3C	20:60:20	9	36.03 \pm 3.53 ^a	29.51 \pm 0.11 ^{cd}	285.15 \pm 1.73 ^d	1.43
CP4C	20:40:40	11	34.76 \pm 2.80 ^a	30.76 \pm 0.86 ^{bc}	276.45 \pm 1.51 ^e	1.45
CP5C	20:50:30	11	35.45 \pm 2.45 ^a	32.57 \pm 0.89 ^b	268.05 \pm 2.28 ^f	1.47
CP6C	20:60:20	11	36.56 \pm 3.61 ^a	36.43 \pm 0.11 ^a	259.27 \pm 0.36 ^g	1.51
CP7C	0:50:50	9	33.36 \pm 3.94 ^a	27.80 \pm 0.33 ^{de}	374.84 \pm 2.19 ^a	1.14

^aValues in the same of column with different superscripts are significantly different ($p < 0.05$).

their porous structure and adsorption capability.¹⁶ They can be engineered to meet specific needs. A diverse range of chemical and natural polymers can be strategically manipulated to achieve their desired properties.^{17,18} Different hydrogels, such as poly(*N*-vinyl-2-pyrrolidone)/(acrylic acid-*co*-styrene) hydrogel,¹⁵ paramagnetic poly(styrene-*co*-acrylamide) hydrogel,¹⁹ Arabic gum-*graft*-polyamidoxime/CuFe₂O₄ nanocomposite hydrogel,²⁰ and covalent organic frameworks functionalized with graphene,^{10,21} have been reported for the remediation of pesticides. Although several hydrogels are employed for pesticide adsorption, investigations concerning the utilization of raw cellulose-based hydrogels for the removal of pesticides, such as malathion, have yet to be documented.

Cellulose is one of the most abundant polymers in nature. Synthesizing a biodegradable hydrogel from raw cellulose with minimal processing and chemical usage, while demonstrating its excellent pesticide adsorption performance, can promote the development of adsorption materials. Poly(vinyl alcohol) (PVA), a synthetic biodegradable polymer, possesses favorable attributes for hydrogel formation, including strong adhesion, water solubility, and ease of binding to material surfaces.²² Chang et al.²³ and Ban et al.²⁴ synthesized cellulose/PVA hydrogels. They observed that the addition of PVA enhanced the swelling degree of cellulose hydrogels. β -cyclodextrin (β -CD) has been investigated for creating hydrogels aimed at encapsulating and controlling the release of active substances, as well as for adsorption purposes. β -CD is characterized by its doughnut-shaped ring structure, featuring a hydrophilic outer surface to form hydrogen bonds, alongside a hydrophobic central cavity for compound inclusion to enhance the adsorption capacity. Zhang et al.²⁵ synthesized β -CD/cellulose hydrogels using epichlorohydrin (ECH) as the cross-linker. Their results suggest that β -CD-containing hydrogels can effectively encapsulate hydrophobic compounds. In addition, Sharma et al.²⁶ synthesized a biodegradable β -cyclodextrin/poly(vinyl alcohol)/chitosan hydrogel, which showed a good adsorption efficiency for bentazon pesticide. Thus, we hypothesize that cross-linking β -CD with raw cellulose and

PVA can produce high-adsorption ability hydrogels with both hydrophilic and hydrophobic domains, enhancing their capacity to adsorb amphiphilic compounds like malathion.

In this study, environmentally friendly cellulose-based hydrogels were synthesized and evaluated for malathion adsorption. PVA and β -CD served as copolymers, with biobased ECH as the cross-linker. The aim was to assess how the cellulose-to-PVA ratio and the ECH content influence the key properties of the hydrogels and their ability to adsorb malathion. These properties include moisture content, gel content, swelling ratio, density, and biodegradability. Analytical techniques, such as Fourier transform infrared (FTIR) spectroscopy, ζ -potential, X-ray diffraction (XRD), thermogravimetric analysis (TGA), X-ray photoelectron spectroscopy (XPS), nuclear magnetic resonance (NMR) spectroscopy, N₂ sorption analysis, and field emission scanning electron microscopy (FESEM), were employed to characterize the hydrogels and substantiate the data on their properties and adsorption capabilities.

2. RESULTS AND DISCUSSION

2.1. Properties of β -CD/Cellulose/PVA Hydrogels. The synthesis and freeze-drying of β -CD/cellulose/PVA hydrogels resulted in the products depicted in Figure 1, and their properties are summarized in Table 1. The moisture content of the hydrogels was not significantly affected by variations in the cellulose/PVA ratio or the amount of ECH used. For instance, the water activity of the CP1C sample was 0.307, below the threshold of 0.6, suggesting microbial stability of the synthesized hydrogel.²⁷ An increase in the cellulose-to-PVA ratio and ECH content led to a higher gel content, indicative of a denser cross-linked structure.^{28,29} Correspondingly, this result aligns with the observed increase in the density. Conversely, the swelling ratio decreased with a higher cellulose-to-PVA ratio and ECH content, attributed to the more densely cross-linked structure limiting the expansion and water adsorption capacity.^{28,29} Nonetheless, an increased PVA content enhanced the swelling ratio, indicating the predom-

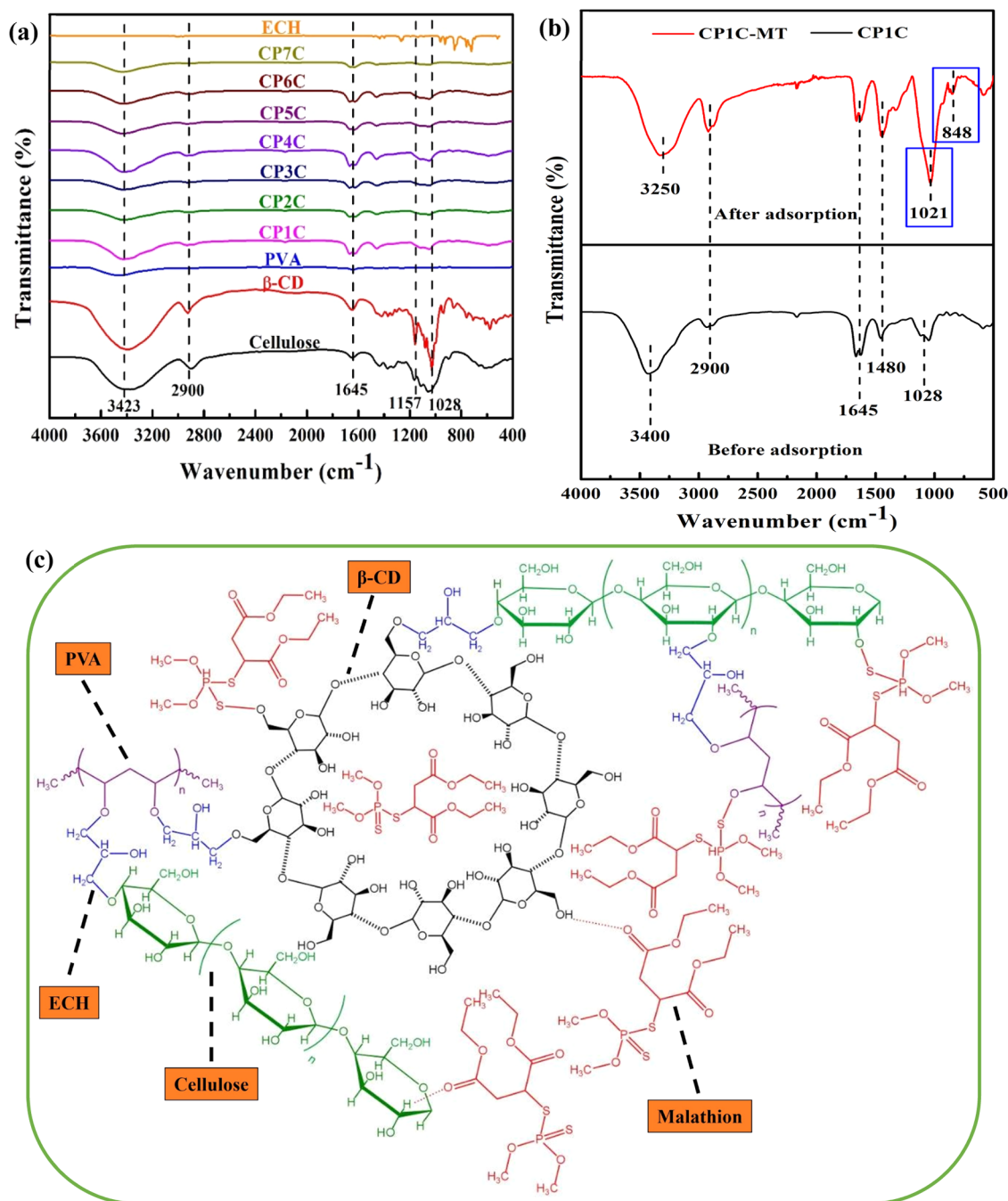


Figure 2. (a) FTIR spectra of cellulose, β -CD, PVA, ECH, and β -CD/cellulose/PVA hydrogels, (b) FTIR spectra of β -CD/cellulose/PVA hydrogel (CP1C) before and after malathion adsorption, and (c) plausible adsorption mechanism of the adsorption.

inant effect of hydrophilicity of PVA over cellulose in this context.²³

Interestingly, the moisture content and gel content were comparable between hydrogels with and without β -CD (CP1C and CP7C, respectively). This suggests that the presence of β -CD did not significantly alter these properties. However, a marked difference was observed in the swelling ratio and density between CP1C and CP7C samples; the hydrogel without β -CD showed a higher swelling ratio, which can be attributed to its lower density allowing for greater expansion and swelling capacity.^{28,29} These findings indicate that β -CD reduces the hydrophilicity of the hydrogels, affecting their swelling behavior.

2.2. Structure of β -CD/Cellulose/PVA Hydrogels.

Figure 2a presents the FTIR spectra of β -CD, cellulose, PVA, ECH, β -CD/cellulose/PVA hydrogels (CP1C–CP6C), and the cellulose/PVA hydrogel (CP7C). The 2900 cm^{-1} peak, corresponding to the C–H bond stretching vibration, was observed in both β -CD and cellulose, whereas the 1645 cm^{-1} peak associated with the H–O–H bending vibration was also noted. The C–O–C and C–OH stretching vibrations were identified at 1157 and 1028 cm^{-1} , respectively, with a broad peak at 3423 cm^{-1} attributable to the hydroxyl group (OH) stretching vibration, present in β -CD, cellulose, and PVA. These peaks confirmed the presence of β -CD, cellulose, and PVA in the hydrogels.^{30,31} The absence of the 1028 cm^{-1}

peak in the CP7C hydrogel indicated the lack of an β -CD. A reduced intensity of the 3423 cm^{-1} peak in the hydrogels, compared to pure β -CD and cellulose, suggests a decrease in hydroxyl groups and hydrogen bonding, resulting from the cross-linking reaction between ECH and the hydroxyl groups of β -CD, cellulose, and PVA.^{18,30} After the adsorption of malathion (MT), the sample was labeled CP1C-MT, as depicted in Figure 2b. It was observed that the peaks of CP1C-MT shifted compared to those of CP1C. The characteristic peak of malathion at 1021 cm^{-1} , associated with the vibration of P-OCH₃ group³² and the band at 850 cm^{-1} , indicating the bond formation of S-OR group, was evident.³³ These FTIR results confirmed the adsorption of malathion on the hydrogel. Additionally, the ζ -potentials of CP1C and CP7C hydrogels before adsorption were found to be -10.61 ± 0.51 and -10.08 ± 0.43 mV, respectively, while those after malathion adsorption were -8.02 ± 0.32 and -8.98 ± 0.27 mV, respectively. This observation indicated that the hydrogels exhibited net negative charges on their surfaces before adsorption, with the adsorption of malathion resulting in a reduction of the net negative ζ -potential on the hydrogel surface. These changes in ζ -potential between before and after adsorption illustrate the occurrence of electrostatic interaction between the hydrogel and malathion, with the hydrogel containing β -CD (CP1C) showing a slightly higher electrostatic interaction than the hydrogel without β -CD (CP7C). Figure 2c presents the plausible adsorption mechanism of malathion. The adsorption possibly involved the formation of covalent bonds between sulfur (S) atoms in malathion and oxygen (O) atoms of β -CD, cellulose, PVA, and ECH on the hydrogel.³⁴ Additionally, the C=O groups in malathion could form hydrogen bonds with the OH groups of β -CD, cellulose, PVA, and ECH, while electrostatic interactions between the C=O groups in malathion and hydrogen (H) atoms of cellulose may occur.²⁶ Furthermore, the hydrophobic groups such as P-OCH₃ and OC₂H₅ groups of malathion could be trapped within the cavity of β -CD through hydrophobic interactions.³⁵ The presence of various functional groups on the synthesized hydrogel contributed to its high adsorption capacity for malathion.

Figure S1 depicts the XRD patterns of β -CD, cellulose, PVA, and hydrogels. The crystalline nature of β -CD is indicated by peaks at 2θ of 11° and 12.5° . Cellulose crystallinity is represented by diffraction peaks at 2θ of 16° , 22.5° , and 34.2° , corresponding to the (010), (002), and (040) crystalline planes, respectively. A peak at approximately 19.8° reflects the crystallinity of PVA, associated with the (101) crystalline plane, confirming PVA has semicrystalline nature. Notably, the hydrogels did not exhibit any crystalline peaks for β -CD, cellulose, or PVA. This absence is likely due to the chemical cross-linking among the hydroxyl groups of β -CD, cellulose, and PVA, which impedes the crystallization of these components, resulting in amorphous hydrogel structures.^{23,36} The amorphous structure of hydrogels implies that they exhibit swelling behavior and possess adsorption ability.³⁷

Figure 3a illustrates the thermal degradation behavior of the hydrogels showing two major mass loss regions. The first degradation step, occurring between 180 and 330 $^\circ\text{C}$, is attributed to the pyrolysis of cellulose and the degradation of PVA, primarily through dehydration reactions leading to polylene formation.^{36,38} This phase accounts for approximately 60% of the mass loss. The second degradation step, beyond 330 $^\circ\text{C}$, involves the decomposition of the carbon backbone

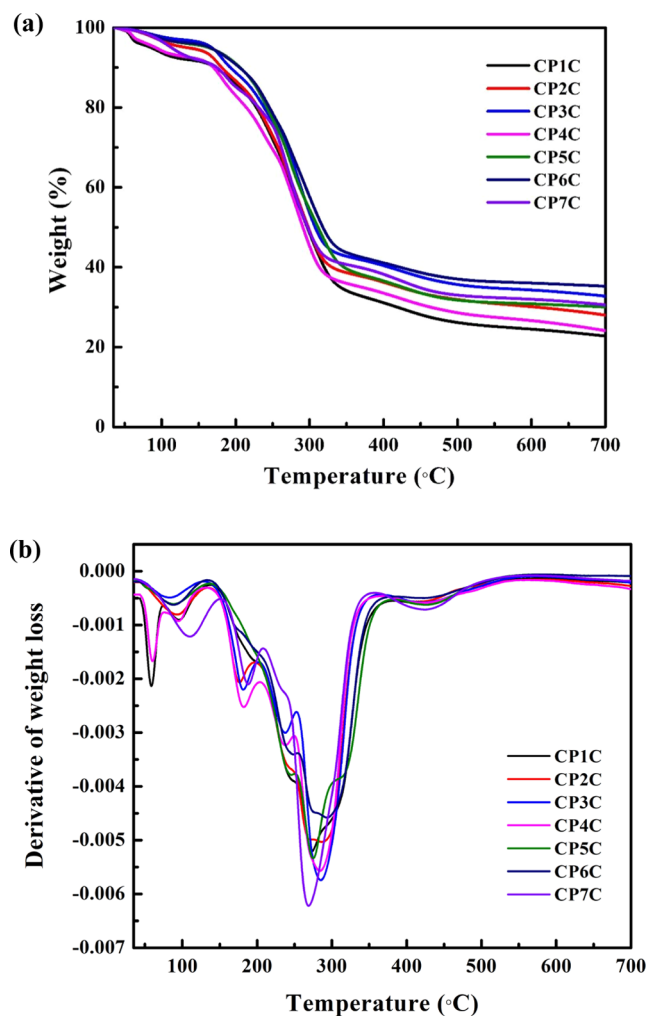


Figure 3. (a) TG and (b) DTG curves of β -CD/cellulose/PVA hydrogels.

within the hydrogels.^{36,39} The mass residue percentage above 500 $^\circ\text{C}$ increased with a higher cellulose-to-PVA ratio and ECH content, indicating enhanced thermal stability due to increased intermolecular hydrogen bonding between PVA and cellulose.^{36,40} Figure 3b shows the DTG degradation profiles of hydrogel samples. It was found that the maximum peak, where the greatest mass loss occurs, for all samples was at temperatures close to 300 $^\circ\text{C}$.

Figure S2a presents the XPS full spectra of the CP1C sample before and after malathion adsorption, showing carbon (C) and oxygen (O) as the main elements. Figure S2b details the high-resolution scan of the C_{1s} spectra for the CP1C sample, revealing four Gaussian peaks corresponding to different carbon-containing functional groups: C–C at 284.6 eV, C–O at 285.8 eV, O–C–O at 286.6 eV, and C=O at 288 eV. The intensities of the C–O and C=O peaks increased after malathion adsorption, indicating an interaction with malathion molecules.^{41,42} Figure S2c shows the O 1s spectrum of CP1C, which can be split into three peaks representing C=O, C–OH, and C–O–C bonds at 530.8, 532.2, and 533.3 eV, respectively.^{43–45} Postadsorption, an increase in C=O and C–O–C intensities and a decrease in C–OH intensities were observed, suggesting that hydroxyl groups were replaced by carbonyl and ether groups of malathion on the hydrogel surface.⁴¹

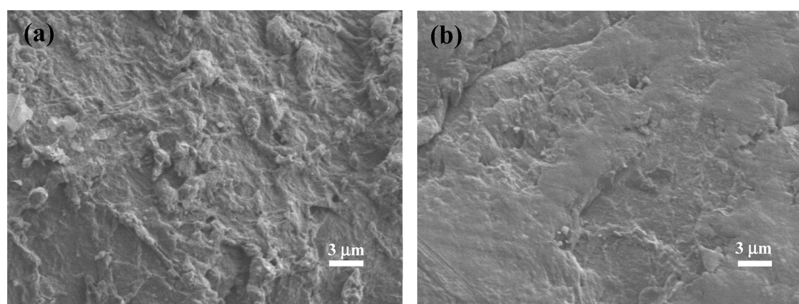


Figure 4. FESEM images of β -CD/cellulose/PVA hydrogels: (a) CP1C and (b) CP7C.

Figure S3 depicts the N_2 adsorption–desorption curve of the CP1C hydrogel. The CP1C hydrogel exhibited a type IV isotherm with a hysteresis loop of type H1, as classified by IUPAC. This indicated a mesoporous structure for the hydrogel, with an average pore size of approximately 32.4 nm, a BET surface area of $3.80 \text{ m}^2 \text{ g}^{-1}$, and a total pore volume of $0.031 \text{ m}^3 \text{ g}^{-1}$.^{46,47}

Figure 4 illustrates the morphology of β -CD/cellulose/PVA hydrogels prepared under CP1C and CP7C conditions. All displayed hydrogels exhibited smooth surfaces with some visible cellulose fibers. The pores were not observable by using the SEM technique. The synthesized hydrogels could be categorized as nonporous hydrogels, which have only small pores that are typically in the range of tens of nm for the alginate gel network.⁴⁸ This finding was consistent with the results obtained from the analysis of hydrogel pore size using the N_2 -adsorption–desorption method. Jayaramudu et al.⁴⁰ observed similar characteristics in PVA/cellulose hydrogels, noting their smooth and nonporous surfaces. It is important to acknowledge that while such biobased hydrogels like cellulose/PVA may have less porous structures and potentially lower adsorption capabilities compared to chemically synthesized hydrogels, they offer the advantages of being more easily degradable and environmentally friendly.⁴⁹

Figure 5 presents the biodegradation profile of the CP1C hydrogel through soil burial, revealing a rapid degradation rate initially with a 64.75% mass loss in the first week. The degradation continued over time, with the total mass loss

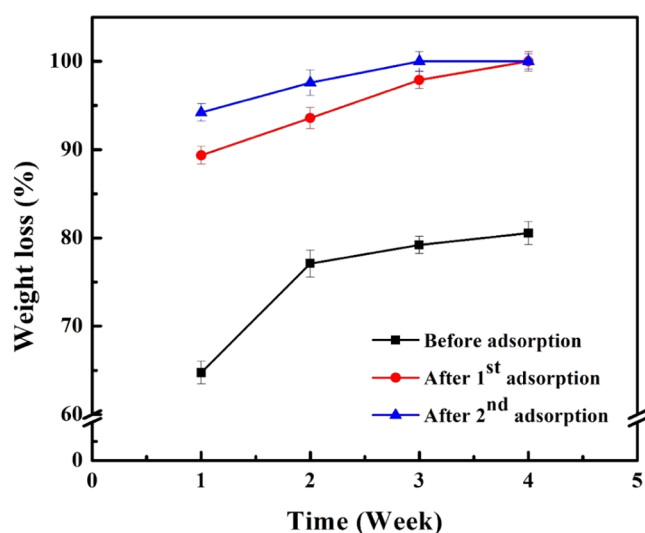


Figure 5. Biodegradation of CP1C sample in natural conditions by the soil burial method for 4 weeks.

reaching about 80.55% after 4 weeks. The hydrogel exhibited rapid degradation following malathion adsorption. After the first cycle, it lost nearly 90% of its mass within the first week and completely degraded within 4 weeks. Notably, the second adsorption cycle further accelerated degradation. The hydrogel lost nearly 95% of its mass within the first week and degraded completely within just 3 weeks.

This indicates the high biodegradability of the biobased materials used in the hydrogel, such as cellulose, β -CD, and ECH, which serve as cross-linking agents, and PVA, a synthetic polymer known for its biodegradable properties. The combined use of these materials in hydrogel synthesis contributes to its rapid natural decomposition.

2.3. Effect of Contact Time on Malathion Adsorption Capability. The adsorption rate is a critical measure of an adsorbent's performance. Figure 6 illustrates the adsorption

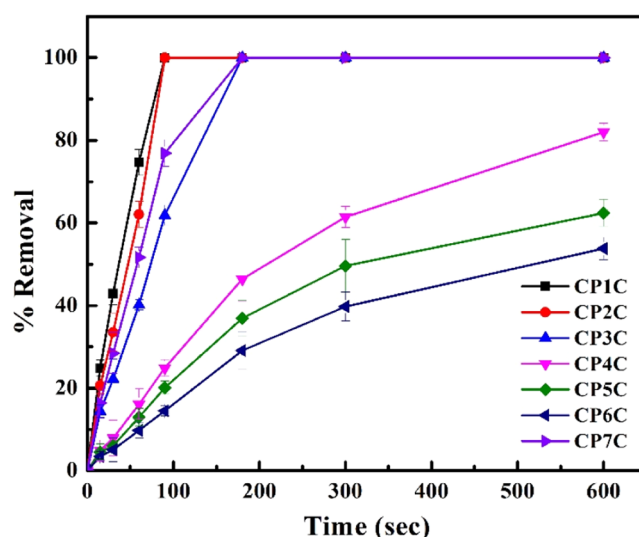


Figure 6. Adsorption capacities of malathion on CP1C–CP7C. 0.1 g portion of dried β -CD/cellulose/PVA hydrogels, 70 mL of malathion solution, and an initial malathion concentration of 50 mg L^{-1} were used.

capacities for malathion across all β -CD/cellulose/PVA hydrogels (CP1C–CP7C) at an initial concentration of 50 mg L^{-1} . As anticipated, the adsorption percentage of malathion increased with longer contact times. However, hydrogels synthesized under different conditions demonstrated varying adsorption capacities. Those prepared with 9 mL of ECH showed significantly greater adsorption capabilities than those with 11 mL of ECH, due to the latter's denser hydrogel structures, which impeded adsorption. Similarly, an increase in

cellulose content reduced adsorption capacity, as higher cellulose levels resulted in denser and less flexible hydrogels, leading to decreased swelling ratios and adsorption capacities.^{28,29}

The hydrogel with the highest malathion adsorption capability was CP1C, closely followed by CP2C. Remarkably, both of these hydrogels could completely adsorb malathion within just 90 s. The CP7C sample, lacking β -CD, achieved complete malathion adsorption in approximately 3 min. The adsorption rate for malathion on CP7C was lower than on CP1C, indicating that β -CD presence enhances the hydrogel's malathion adsorption rate. This enhancement is likely due to the entrapment of malathion's hydrophobic regions within the hydrophobic cavity of β -CD, facilitating faster adsorption onto the hydrogel.²⁵

2.4. Effect of Adsorbent Dosage on Malathion Adsorption Capability. Figure 7 illustrates the impact of

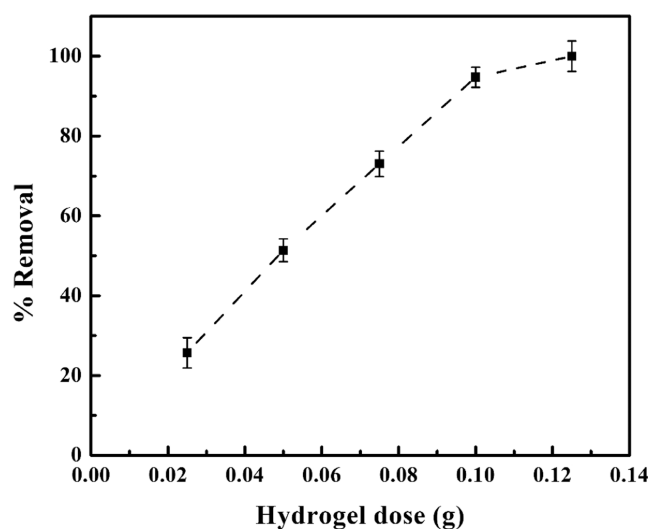


Figure 7. Effect of adsorbent dosage on malathion adsorption capacity of β -CD/cellulose/PVA hydrogel (CP1C) at a contact time of 10 min. 0.025–0.125 g of dried β -CD/cellulose/PVA hydrogel, 70 mL of malathion solution, and an initial malathion concentration of 500 mg L⁻¹ were used.

the adsorbent dosage on the malathion adsorption capacity of the CP1C sample. The dosage was varied within the range of 0.025–0.125 g, utilizing an initial malathion concentration of 500 mg L⁻¹. The adsorption experiments were conducted at room temperature with continuous shaking for 10 min to achieve equilibrium conditions. As observed, the percentage removal of malathion increased with higher adsorbent dosages. This result can be attributed to the introduction of more active sites on the hydrogel surface, consequently enhancing the adsorption of malathion.^{26,50}

2.5. Effect of pH on Malathion Adsorption Capability.

The pH of the solution is a critical factor in the removal of malathion,⁵¹ as it affects both the degradability of the adsorbate and the adsorption capacity.¹⁴ Consequently, understanding the impact of pH on malathion's adsorption capacity is essential. In the study, the pH range tested was between 3 and 9, with adjustments made using 0.1 M NaOH or 0.1 M HCl to achieve the desired pH levels. This examination helps in determining the optimal pH conditions for maximizing the malathion adsorption efficiency.

Figure 8 depicts the adsorption behavior of malathion by the CP1C hydrogel sample across pH levels 3–9, with an initial

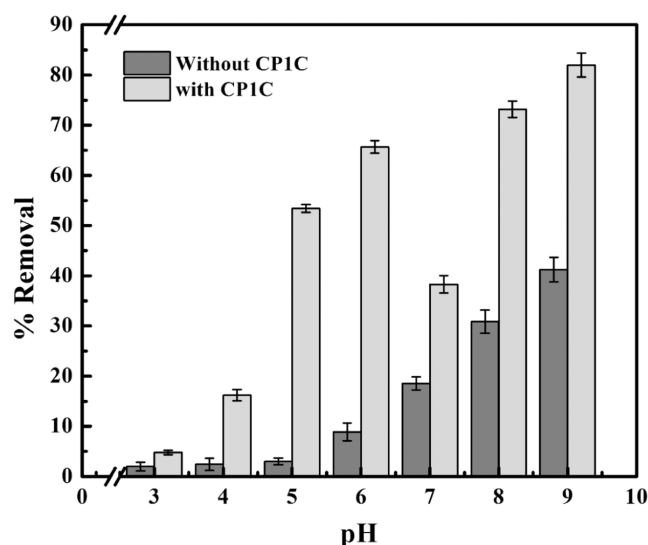


Figure 8. Effect of pH on malathion adsorption capacity of β -CD/cellulose/PVA hydrogel (CP1C) at a contact time of 30 s. 0.1 g of dried β -CD/cellulose/PVA hydrogel, 70 mL of malathion solution, and an initial malathion concentration of 50 mg L⁻¹ were used.

malathion concentration of 50 mg L⁻¹ and a contact time of 30 s. To assess malathion's stability under different pH conditions, control experiments without hydrogel were performed. The results showed that malathion degradation was higher in solutions at pH 8–9, indicating rapid degradation under alkaline conditions.⁵² The hydrogel adsorbents enhanced malathion removal more effectively under alkaline conditions than under acidic conditions. At a weakly acidic pH of 6, the hydrogel significantly increased malathion removal from 10 to 70%, demonstrating its high adsorption efficiency. In contrast, at pH 7, the adsorption capacity decreased, likely due to diminished electrostatic interactions in neutral conditions.¹⁰ In alkaline conditions, the hydrogel's impact on malathion removal was less marked, with the percentage removal increasing from about 40–80% at pH 9. This is mainly attributed to the considerable degradation of malathion in alkaline environments, which left less of the compound available for adsorption. Consequently, the difference in malathion removal using the hydrogel was minimal under these conditions, illustrating the complex interplay between the chemical stability and adsorption efficiency in varying pH environments.

2.6. Effect of Initial Concentration on Malathion Adsorption.

Figure 9 illustrates how the initial concentration of malathion influences its equilibrium adsorption capacity and percentage removal by using the CP1C hydrogel sample. The study was conducted with initial malathion concentrations ranging from 500 to 1000 mg L⁻¹, and equilibrium was achieved within a 10 min contact time. The equilibrium adsorption capacities (q_e) for malathion were found to be 337.45 mg L⁻¹ at 500 mg L⁻¹, 400.81 mg L⁻¹ at 600 mg L⁻¹, 467.19 mg L⁻¹ at 700 mg L⁻¹, 528.18 mg L⁻¹ at 800 mg L⁻¹, and 656.41 mg L⁻¹ at 1000 mg L⁻¹ initial concentrations, respectively. The q_e value increased as the initial malathion concentration rose, which can be attributed to the enhanced concentration gradient serving as the driving force for mass

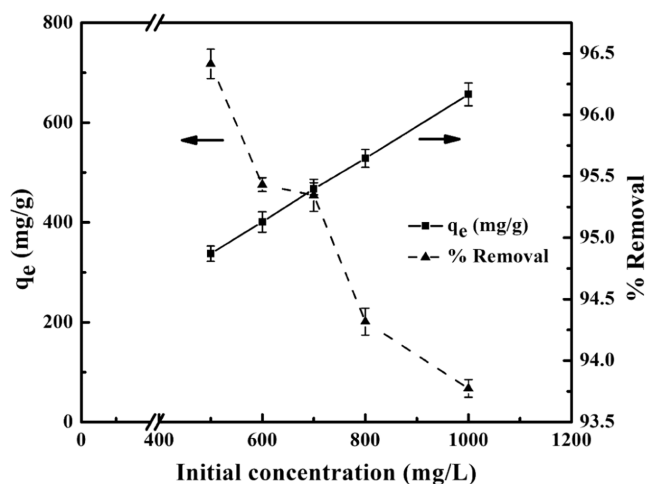


Figure 9. Effect of initial malathion concentration on adsorption capacity of β -CD/cellulose/PVA hydrogel (CP1C). 0.1 g of dried β -CD/cellulose/PVA hydrogel and 70 mL of malathion solution were used.

transfer. Conversely, the percentage of malathion removal declined with increasing initial concentration, as the adsorption sites approached saturation, limiting the capacity for additional adsorption.^{53,54}

2.7. Effect of Temperature on Malathion Adsorption.

Figure 10 depicts the impact of temperature on the percentage

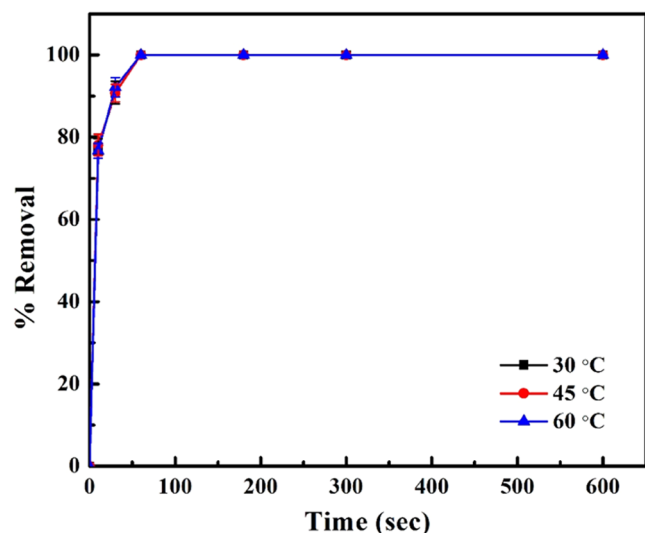


Figure 10. Effect of temperature on the adsorption capacity of β -CD/cellulose/PVA hydrogel (CP1C). 0.1 g of dried β -CD/cellulose/PVA hydrogel, 70 mL of malathion solution, and an initial malathion concentration of 50 mg L⁻¹ were used.

removal of malathion by the CP1C sample at 30, 45, and 60 °C. The experiments were conducted with initial concentrations of 50 mg L⁻¹ and contact times ranging from 0 to 10 min. Interestingly, the results indicated that the percentage of removal of malathion remained consistent across different temperatures. This suggests that the temperature has no effect on the malathion adsorption capacity of the hydrogel.

2.8. Adsorption Isotherms of β -CD/Cellulose/PVA Hydrogels. The malathion adsorption isotherms for β -CD/cellulose/PVA hydrogels are illustrated in Figure 11a,b, representing the Langmuir and Freundlich adsorption models,

respectively. The parameters for these models are listed in Table 2. The adsorption behavior of malathion on β -CD/cellulose/PVA hydrogels aligned more closely with the Freundlich isotherm model, as evidenced by consistently higher R^2 values compared with those for the Langmuir model. This suggests that the adsorption of malathion onto the hydrogels involved a multilayer process on heterogeneous adsorbent surfaces, characteristic of the Freundlich adsorption isotherm model.⁵⁵

2.9. Adsorption Kinetics of Malathion on β -CD/Cellulose/PVA Hydrogels.

The kinetics of malathion adsorption on β -CD/cellulose/PVA hydrogels were analyzed using pseudo-first-order, pseudo-second-order, and intraparticle diffusion model equations, as shown in Figure 12a–c, respectively. The parameters for these kinetic models are detailed in Table 3. The adsorption kinetics of malathion on the hydrogels aligned most closely with the intraparticle diffusion model, as indicated by the high R^2 values of 0.9346, 0.9944, and 0.9968 at initial malathion concentrations of 500, 800, and 1000 mg L⁻¹, respectively. This suggests that the adsorption process is likely governed by mass diffusion, with the intraparticle diffusion model providing the best description of the kinetics involved.^{55,56}

2.11. Reusability Evaluation. Figure 13 shows the malathion adsorption capacity of the CP1C sample across the first and second adsorption–desorption cycles, revealing that the reused hydrogel had a reduced adsorption capacity for malathion. This reduction is likely due to structural changes or denaturation occurring during the desorption and drying processes, which are common limitations in biobased hydrogels.

Table 4 compares the maximum adsorption capacity (q_m) for malathion among various adsorbents reported in other studies. The data highlight that the β -CD/cellulose/PVA hydrogel showed superior malathion adsorption capacity, with a q_m of 1111.11 mg g⁻¹. This illustrates that cellulose-based hydrogel, functionalized with hydrophilic and hydrophobic sites, can enhance the adsorption capacity of malathion. However, the limitation of using this synthesized hydrogel was due to its low reusability. Therefore, further improvement in the stability of these biodegradable β -CD/cellulose/PVA hydrogel can enhance its potential for practical application.

3. CONCLUSIONS

The β -CD/cellulose/PVA hydrogels were successfully synthesized through cross-linking with biobased epichlorohydrin, leading to significant changes in their physical properties. The gel content and density increased, whereas the swelling ratio decreased with a higher cellulose/PVA ratio and ECH content. Hydrogels containing β -CD showed notably lower swelling ratios than those without β -CD. The ECH content had a more pronounced impact on both the gel content and the malathion adsorption capacity compared to the cellulose-to-PVA ratio. Additionally, the inclusion of β -CD enhanced the malathion adsorption capacity of the hydrogels. The optimal formulation, with a β -CD/cellulose/PVA ratio of 20:40:40 and 9 mL of ECH (CP1C), achieved the highest adsorption efficiency, completing malathion adsorption at an initial concentration of 50 mg L⁻¹ within 90 s. The CP1C hydrogel showed an equilibrium adsorption capacity of 656.41 mg g⁻¹ at an initial malathion concentration of 1000 mg L⁻¹. The adsorption process predominantly followed the Freundlich isotherms, indicative of multilayer adsorption, and the intraparticle

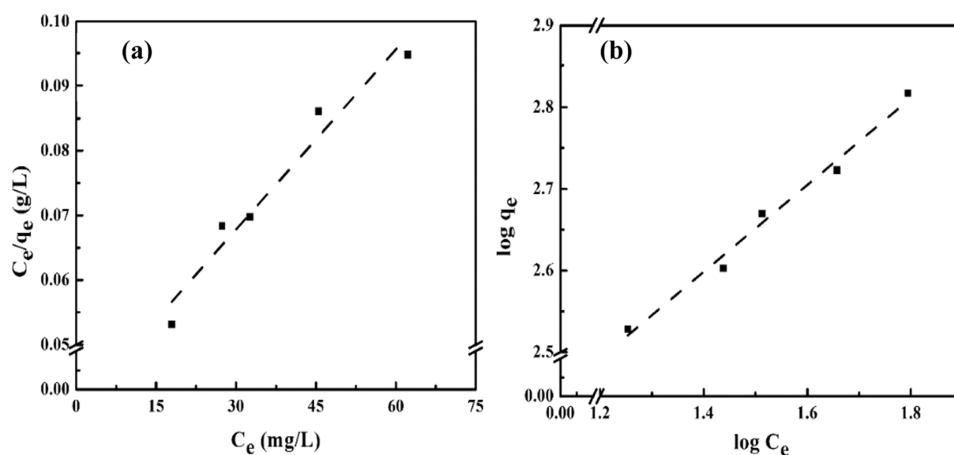


Figure 11. Isotherms of malathion adsorption on β -CD/cellulose/PVA hydrogel (CP1C). (a) Langmuir isotherm and (b) Freundlich isotherm. 0.1 g of dried β -CD/cellulose/PVA hydrogel and 70 mL of malathion solution were used.

Table 2. Parameters of Isotherm Models for Malathion Adsorption Using the β -CD/Cellulose/PVA Hydrogel (CP1C)

sample	Langmuir isotherm			Freundlich isotherm		
	q_m (mg g^{-1})	b (L mg^{-1})	R^2	K_F ($(\text{mg g}^{-1})(\text{L mg}^{-1})^{1/n}$)	$1/n$	R^2
CP1C	1111.11	0.0225	0.9579	71.53	0.53	0.9864

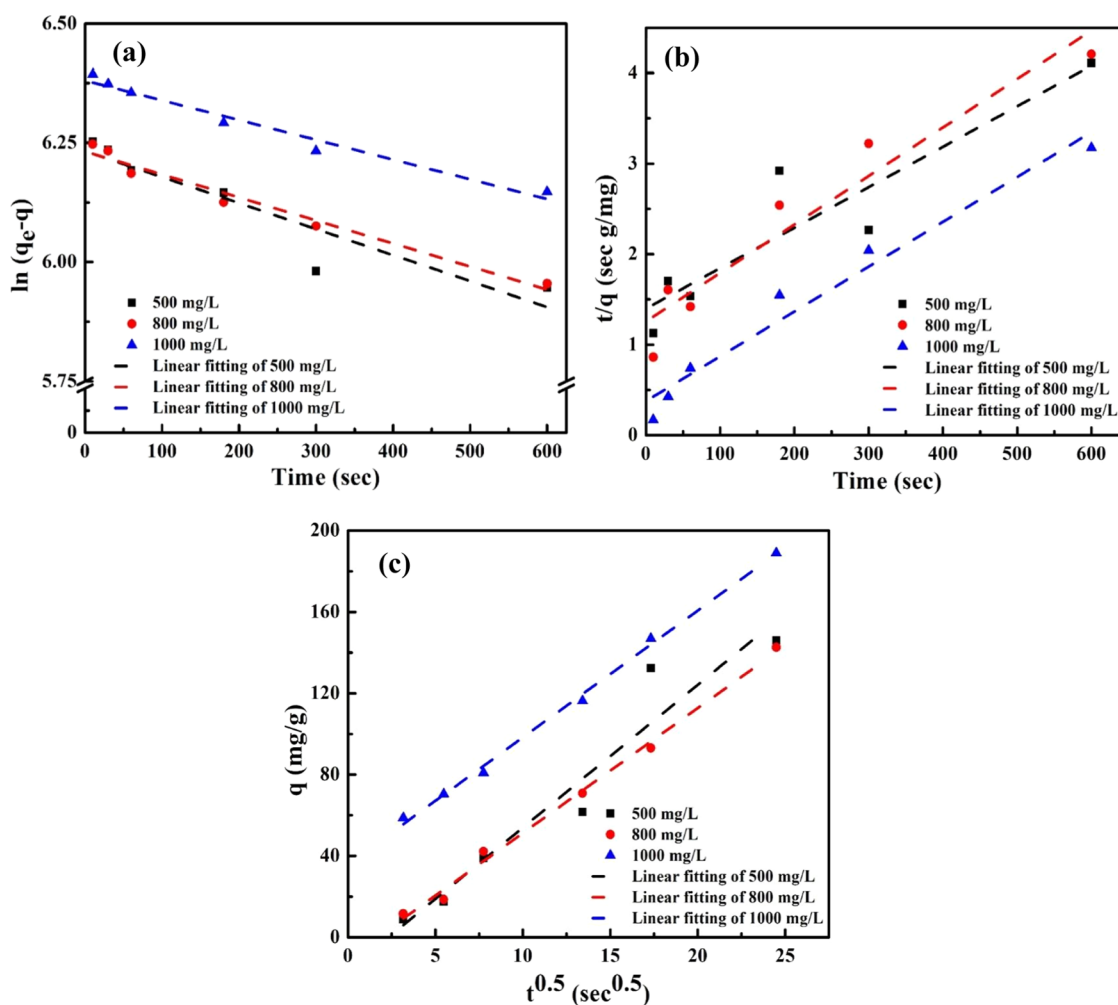
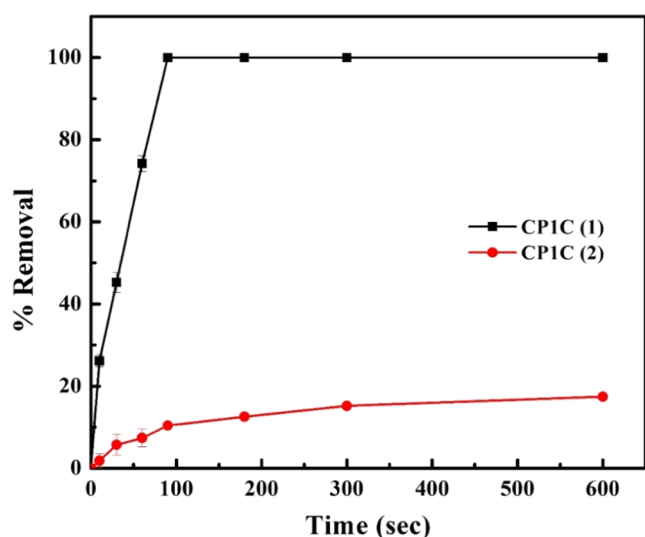


Figure 12. Kinetic modeling results for malathion adsorption on β -CD/cellulose/PVA hydrogel (CP1C), showing (a) pseudo-first-order kinetic model, (b) pseudo-second-order kinetic model, and (c) intraparticle diffusion model. Experiments were conducted using 0.1 g of the dried β -CD/cellulose/PVA hydrogel and 70 mL of malathion solution.

Table 3. Parameters of Kinetic Models for Malathion Adsorption Using the β -CD/Cellulose/PVA Hydrogel (CPIC)

model parameter	initial malathion concentration (mg L ⁻¹)		
	500	800	1000
$q_{e(\text{exp.})}$	337.45	528.18	656.41
Pseudo-first-order			
$q_{e(\text{calcd})}$ (mg g ⁻¹)	236.56	508.77	590.16
k_1 (s ⁻¹)	0.0023	0.0012	0.00092
R^2	0.8835	0.9734	0.9719
Pseudo-second-order			
$q_{e(\text{calcd})}$ (mg g ⁻¹)	222.22	185.18	204.08
k_2 (g mg ⁻¹ s ⁻¹)	1.45×10^{-5}	2.32×10^{-5}	6.37×10^{-5}
R^2	0.8517	0.9288	0.9659
Intraparticle Diffusion			
k_p (mg g ⁻¹ s ^{-0.5})	7.0181	6.1426	6.2328
C_i	-16.184	-10.142	35.988
R^2	0.9346	0.9944	0.9968

**Figure 13.** Adsorption capacities of malathion on CPIC during the first and second adsorption–desorption cycles using 0.1 g of dried β -CD/cellulose/PVA hydrogels, 70 mL of malathion solution, and an initial malathion concentration of 50 mg L⁻¹.

diffusion model best described the experimental adsorption kinetics, suggesting a diffusion-dominant adsorption process.

4. MATERIALS AND METHODS

4.1. Materials. Food-grade cellulose powder (Vitacel LC 200) was obtained from Rama Production Co., Ltd., Bangkok, Thailand. Biobased epichlorohydrin (ECH, 99%) was provided by Advanced Biochemical (Thailand) Co., Ltd., Rayong, Thailand. Sodium hydroxide (NaOH, 97%) and urea (crystalline, 99%) were procured from Elago Enterprises Pty Ltd., New South Wales, Australia. β -Cyclodextrin (β -CD, 98%) was sourced from Chanjao Longevity Co., Ltd., Bangkok, Thailand. Poly(vinyl alcohol) (PVA, 86–90% hydrolyzed) was acquired from Chem-Supply Pty Ltd., Gillman, Australia. Hydrochloric acid (HCl, 37%) was purchased from Qchemical Co., Ltd. (QRC), New Zealand. Acetonitrile (ACN) and methanol (MeOH) of high-performance liquid chromatography (HPLC) grade (99%) were purchased from Honeywell Co., Ltd., Seoul, South Korea. The malathion standard (MT, 98.33%) was procured from LGC Labor GmbH, Augsburg, Germany.

4.2. β -CD/Cellulose/PVA Hydrogels Synthesis. Approximately 4 g of cellulose powder was dispersed in 96 g of a solution containing 6% NaOH and 4% urea (wt %). This mixture was stirred for 5 min before being stored in a freezer at -20 °C for 12 h. After being frozen, the cellulose solution was thawed at room temperature until it became transparent. PVA was dissolved in the same solvent mixture as cellulose to achieve a 4 wt % concentration. 20 β -CD was dissolved in a solution of 7% NaOH and 12% urea (wt %) to reach a 4 wt % concentration. Solutions of β -CD, cellulose, and PVA were prepared in various ratios, as detailed in Table 5, and each

Table 5. Reaction Conditions and Compositions of β -CD/Cellulose/PVA Hydrogels

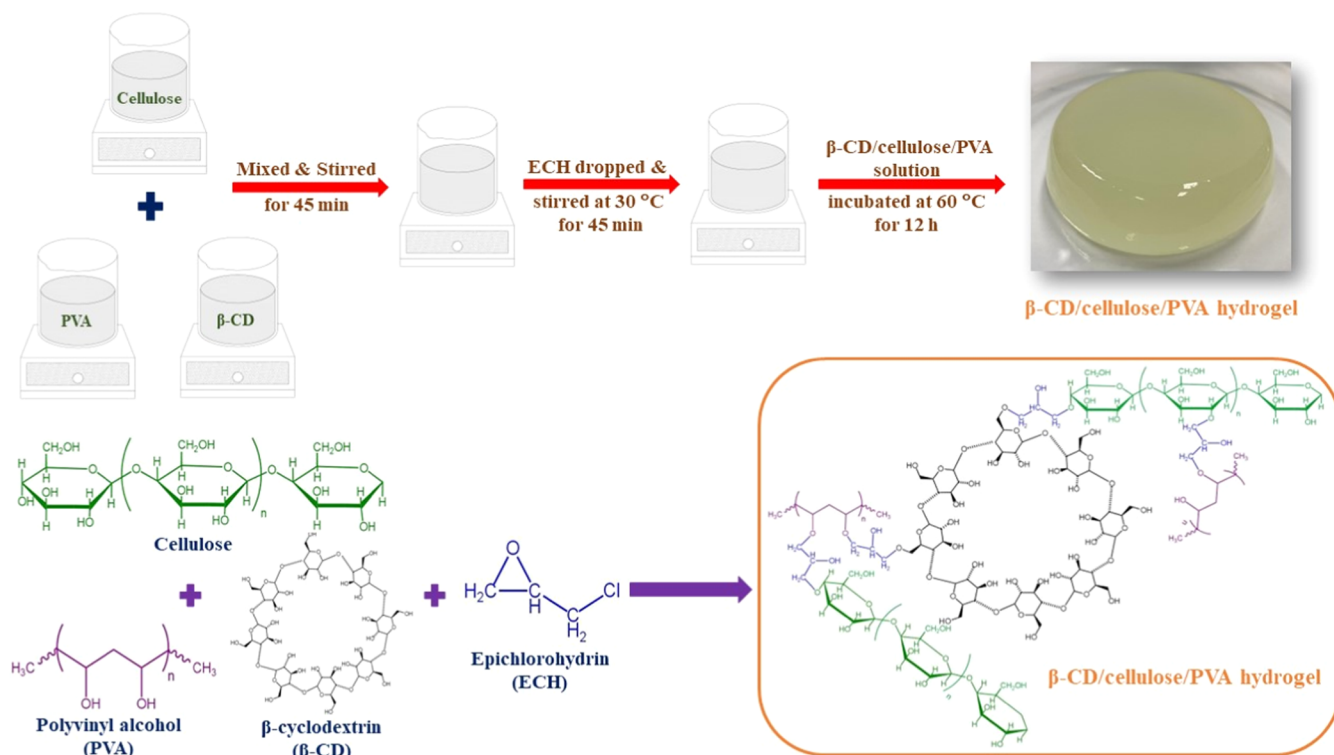
sample	β -CD solution (g) (4 wt %)	cellulose solution (g) (4 wt %)	PVA solution (g) (4 wt %)	volume of ECH (Tomlin)
CP1C	20	40	40	9
CP2C	20	50	30	9
CP3C	20	60	20	9
CP4C	20	40	40	11
CP5C	20	50	30	11
CP6C	20	60	20	11
CP7C	0	50	50	9

mixture was stirred until becoming homogeneous. ECH was then added to each solution, followed by continuous stirring at

Table 4. Comparison of the Maximum Adsorption Capacity (q_m) for Malathion Adsorption on Different Adsorbents

adsorbents	conditions	q_m (mg g ⁻¹)	isotherm	kinetic	refs
β -CD/cellulose/PVA hydrogel	time: 10 min, pH: 6	1111.11	Freundlich	intraparticle diffusion	this work
fly ash	time: 90 min, pH: 4.5	0.726	Langmuir & Freundlich	First-order rate	(Singh et al., 2010) ⁵⁷
de-acidite FF-IP resin	time: 40 min, pH: 6	3.50	Freundlich	Pseudo-second-order	(Naushad et al., 2013) ³⁴
rice husk (RH)	time: 45 min, pH: 6	4.29	Langmuir	Pseudo-second-order	(Kumar et al., 2014) ¹⁴
activated rice husk (ARH)	time: 45 min, pH: 6	16.13	Langmuir	Pseudo-second-order	
powdered activated carbon (PAC)	time: 45 min, pH: 6	21.74	Langmuir	Pseudo-second-order	
activated carbon	time: 15 min, pH: 2.5	32.11		Pseudo-second-order	(Habiba et al., 2015) ⁸
magnetic graphene oxide (MGO)	time: 45 min, pH: 7	43.29	Langmuir	Pseudo-second-order	(Kalantary et al., 2016) ⁵⁸
sodium alginate/biosilicate/magnetite (SABM)	time: 120 min, pH: 7	36.86	Freundlich	Pseudo-second-order	(Hosseini et al., 2019) ⁵
chitosan-alginate (CS-SA) composite	time: 20 min, pH: 7	98.0	Langmuir	Pseudo-second-order	(Sabbagh et al., 2021) ⁵⁹
chitosan-alginate (CS-SA) composite	time: 15 min, pH: 7	58.08	Langmuir	Pseudo-second-order	(Sabbagh et al., 2023) ⁶⁰

Scheme 1. Pictorial Recantation of the Synthesis and Plausible Adsorption Mechanism of the Adsorption



30 °C for 2 h. The mixtures were then incubated at 60 °C for 12 h to facilitate gel formation. Each formed hydrogel was soaked in distilled water for 48 h to leach out unreacted materials, with the water's pH adjusted to 7 using 0.1 M HCl. Synthetic steps and a plausible cross-linking mechanism of the hydrogel are displayed in Scheme 1. The hydrogels were cut into 1 cm cubes, frozen at -20 °C, and subsequently lyophilized in a freeze-dryer (Harvest Right, HRFD-P-M-SS, Salt Lake City, UT) at -40 °C and 0.67 mbar for 24 h.

4.3. Moisture Content Determination. The moisture content (on a dry basis) of each hydrogel sample was determined according to the AOAC method 984.25.⁶¹ Moisture content measurements were conducted in duplicate, and the average value is reported.

$$\text{moisture content (\%)} = \frac{M_i - M_f}{M_f} \times 100 \quad (1)$$

where M_i is the mass of hydrogel prior to drying at 105 °C and M_f is the mass of hydrogel after drying at 105 °C for 72 h.

4.4. Gel Content Determination. Approximately 0.5 g of a hydrogel sample was soaked in 200 mL of distilled water at room temperature for 48 h. The soaked hydrogel was then dried at 105 °C for 24 h before being weighed. The gel content (%) was calculated as follows:⁵⁰

$$\text{gel content (\%)} = \frac{\text{mass of hydrogel after soaking (g)}}{\text{mass of hydrogel before soaking (g)}} \times 100 \quad (2)$$

4.5. Swelling Determination. Approximately 0.1 g of a hydrogel sample was soaked in 200 mL of distilled water at room temperature for 6 h, and then it was weighed. The swelling ratio (%) was calculated as follows:⁵⁰

$$\text{swelling ratio (\%)} = \frac{M_t - M_d}{M_d} \times 100 \quad (3)$$

where M_t is the mass of soaked hydrogel and M_d is the mass of hydrogel prior to soaking.

4.6. Density Determination. The density of a hydrogel sample was determined using an automatic gas pycnometer (Quantachrome, Ultrapyc 1200e, Boynton Beach, FL). Helium gas (99.999% pure) at 21 °C was used for the determination.

4.7. Water Activity Determination. The water activity (a_w) of a hydrogel sample was determined by using a water activity meter (Testo 650, Lenzkirch, Germany) to assess the microbial stability of the sample.

4.8. FTIR Spectroscopy. Functional groups of different hydrogel samples were identified using an FTIR spectrometer (Bruker, Tensor 27, Karlsruhe, Germany). Each hydrogel sample was mixed with KBr powder, and the mixture was compressed into plates for FTIR spectroscopy analysis. The FTIR spectra of the samples were recorded in the wavenumber range of 400–4000 cm^{-1} , with a resolution of 4 cm^{-1} and 64 scans per sample.

4.9. ζ -Potential. ζ -Potential measurements were employed to monitor the surface electric potential of hydrogel samples in both pre- and postadsorption tests to monitor the electrostatic interactions between the hydrogel and malathion. The ζ -potential determination was conducted by utilizing the Zetasizer Nano ZSP instrument (Malvern Instruments, Worcestershire, U.K.). Deionized water was used as a medium for measuring the ζ -potential.

4.10. XRD Analysis. XRD was employed to evaluate the crystalline or amorphous structure of the synthesized hydrogel. XRD was measured using an X-ray diffractometer (Bruker, D8 Advance, Karlsruhe, Germany) with Cu $K\alpha$ radiation ($\lambda = 0.154$ nm). The diffraction patterns were recorded in the 2θ range of 4–40° at a scan rate of 1° min^{-1} .

4.11. TGA Analysis. The thermal stability of the hydrogel was examined by the TGA technique, carried out using a TGA instrument (Mettler Toledo, DSC 1 STARe, Greifensee, Switzerland) under a nitrogen atmosphere at a flow rate of 50 mL min⁻¹. For isothermal degradation analysis, the sample was heated from 30 to 700 °C at a heating rate of 10 °C min⁻¹.

4.12. XPS Analysis. XPS analysis was used to determine the elemental composition on the surfaces of the hydrogel samples. XPS measurements were conducted by utilizing an X-ray photoelectron spectrometer (Kratos, Axis Ultra DLD, San Diego, CA). The peak energies were calibrated by setting the major C 1s peak at 284.5 eV and the O 1s peak at 531 eV.

4.13. Specific Surface Area and Pore Size Distribution Determination. The specific surface area, pore size, and pore volume of the CP1C hydrogel was measured by a sorption analyzer (Micromeritics, 3Flex, Georgia) under a nitrogen atmosphere. The sample was subjected to degassing at 105 °C.

4.14. NMR Analysis. ¹³C NMR spectroscopy was performed to monitor the types of carbon atoms and their bonding patterns using a spectrometer (BRUKER, AVANCE III HD/Ascend 400 WB, Karlsruhe, Germany) operating at 6.0 kHz and 25 °C with a contact time of 6 ms and a pulse delay of 5 s to analyze the chemical groups in the samples.

4.15. FESEM. The morphological structure of each hydrogel sample was examined by using a field emission scanning electron microscope (FESEM, JSM-7600F, JEOL, Tokyo, Japan). Initially, each sample underwent dehydration using a graded ethanol solution. Dehydration involved immersing the samples in ethanol solutions of varying concentrations (30, 50, 60, 80, 95, and 99.8%) for 30 min at each step.⁶² Subsequently, the samples were lyophilized by using a freeze-dryer (Harvest Right, HRFD-P-M-SS, Salt Lake City, UT) at -40 °C and 0.67 mbar for 24 h. Following lyophilization, the samples were crushed into fine powder by using a mortar and pestle, then coated with platinum, and examined using SEM at 5000× magnification, with an accelerating voltage of 1.0 kV.

4.16. Biodegradability Determination. Approximately 0.1 g of the hydrogel sample (dry mass) was buried in soil at a depth of 10 cm and was regularly watered every 2 days to maintain the soil moisture content. The potential for natural landfill biodegradation was assessed by weighing the hydrogel samples weekly for a duration of 4 weeks. At each stage, the samples were rinsed with running tap water to remove any soil residues. Subsequently, they were dried in an oven at 105 °C for 72 h to eliminate all moisture. The biodegradability of the hydrogel samples was determined by assessing the mass loss, calculated as follows:⁶³

$$\text{mass loss (\%)} = \frac{M_0 - M_1}{M_0} \times 100 \quad (4)$$

where M_0 is the dry mass before the test and M_1 is the dry mass after the test at any time.

4.17. Adsorption Performance Determination. Batch adsorption experiments were conducted in 100 mL Erlenmeyer flasks. For each experiment, the concentration of the malathion solution was maintained at 50 mg L⁻¹, with a volume of 70 mL, and the adsorbent dosage was 0.1 g of dry mass. The contact time for malathion adsorption onto the CP1C-CP7C hydrogel samples was varied between 0 and 600 s.

The effects of various relevant parameters, namely, pH, hydrogel dosage, initial concentration of malathion, and

temperature on its adsorption were investigated using the CP1C sample. This sample was selected due to its relatively superior physicochemical properties and its highest malathion adsorption rate and capacity among the samples. The effect of pH was assessed by varying the pH of the malathion solution between 3 and 9. The hydrogel dosage's impact was examined by varying it from 0.05 to 0.125 g dry mass. The initial concentration's effect was explored in the range of 500–1000 mg L⁻¹. The effect of temperature was studied in the range of 30–60 °C. Each adsorbed malathion solution was analyzed by high-performance liquid chromatography (HPLC) to determine the residual malathion content. The HPLC system (Agilent, 1260 Infinity II, Santa Clara, CA) used a UV detector and a C18 column (ACE Excel S:250 × 4.6 mm ID, Avantor, Radnor, PA), operated at a wavelength of 220 nm, a temperature of 35 °C, and a runtime of 35 min. The mobile phase was composed of 50% acetonitrile and 50% water (v/v) with a flow rate of 0.7 mL min⁻¹, and the injection volume was 20 μL.

The percentage of malathion removal (%), adsorption capacity (q), and equilibrium adsorption capacity (q_e) for each β-CD/cellulose/PVA hydrogel were calculated as follows:⁵⁰

$$\text{percentage removal (\%)} = \frac{(C_0 - C_t)}{C_0} \times 100 \quad (5)$$

where C_0 is the initial concentration of malathion solution (mg L⁻¹) and C_t is the concentration of malathion solution at any time during the adsorption (mg L⁻¹).

$$q = \frac{V(C_0 - C_t)}{m} \quad (6)$$

where q is the adsorption capacity at any time during the adsorption (mg g⁻¹), C_0 is the initial concentration of malathion solution (mg L⁻¹), C_t is the concentration of malathion solution at any time during the adsorption (mg L⁻¹), V is the volume of the sample (L), and m is the mass of the added hydrogel adsorbent (g).

$$q_e = \frac{V(C_0 - C_e)}{m} \quad (7)$$

where q_e is the equilibrium adsorption capacity (mg g⁻¹), C_0 is the initial concentration of malathion solution (mg L⁻¹), C_e is the equilibrium concentration of adsorbed malathion solution (mg L⁻¹), V is the volume of the sample (L), and m is the mass of the added hydrogel adsorbent (g).

4.18. Adsorption Isotherms of β-CD/Cellulose/PVA Hydrogels. Adsorption isotherms are typically determined to elucidate the potential interactions between an adsorbent and an adsorbate; these interactions are crucial in establishing the optimal adsorption capacity of an adsorbent at a constant temperature. Adsorption isotherms can be represented in various mathematical forms; however, the chosen form must align with the experimental data. Based on the equilibrium adsorption data for malathion, two different adsorption isotherms, namely, the Langmuir and Freundlich isotherms, were deemed suitable. The Langmuir isotherm equation is commonly utilized for modeling single-layer adsorption on a homogeneous adsorbent surface; once a molecule occupies an adsorption site, no further adsorption can occur at that site. The linear form of the Langmuir isotherm was calculated as follows:^{64,65}

$$\frac{C_e}{q_e} = \frac{1}{bq_m} + \frac{C_e}{q_m} \quad (8)$$

where q_e is the equilibrium adsorption capacity (mg g^{-1}), C_e is the equilibrium concentration of adsorbed malathion solution (mg L^{-1}), q_m is the maximum adsorption capacity at the saturation of a monolayer (mg g^{-1}), and b is the Langmuir constant (L mg^{-1}).

The Freundlich isotherms represent multilayer adsorption on a heterogeneous surface. The linear form of the Freundlich isotherm can be expressed as follows:^{64,65}

$$\log q_e = \log K_F + \frac{1}{n} \log C_e \quad (9)$$

where K_F ($(\text{mg g}^{-1})(\text{L mg}^{-1})^{1/n}$) and n (dimensionless) are the constants of the Freundlich model.

4.19. Adsorption Kinetics of Malathion on β -CD/Cellulose/PVA Hydrogels. Based on the adsorption data for malathion, three adsorption kinetic models were evaluated: the pseudo-first-order model, the pseudo-second-order model, and the intraparticle diffusion model. As previously mentioned, the initial concentration of malathion varied from 500 to 1000 mg L^{-1} . It is noted that the pseudo-first-order model is commonly applied to analyze adsorption data of various adsorbates in aqueous solutions. This model describes the adsorption rate as proportional to the number of unoccupied binding sites on the adsorbent. The pseudo-second-order model, on the other hand, is an adsorption kinetic model that characterizes the adsorption process where chemical bonds (interactions) between the adsorbate and the functional groups on the adsorbent's surface play a significant role in adsorption. The equations for the pseudo-first-order and pseudo-second-order models are provided as eqs 9 and 10, respectively.⁶⁶

$$\ln(q_e - q) = \ln q_e - k_1 t \quad (10)$$

$$\frac{t}{q} = \frac{t}{q_e} + \frac{1}{k_2 q_e^2} \quad (11)$$

where q_e (mg g^{-1}) and q (mg g^{-1}) are the amounts of malathion adsorbed onto hydrogels at equilibrium and at any time during the adsorption (s), respectively. k_1 (s^{-1}) and k_2 ($\text{g mg}^{-1} \text{s}^{-1}$) are the kinetic rate constants of the pseudo-first-order and pseudo-second-order models, respectively.

The intraparticle diffusion model elucidates the adsorption mechanisms, focusing on the diffusion or solute transport from a solution to the solid phase, and is expressed as follows:⁶⁷

$$q = k_p t^{0.5} + C \quad (12)$$

where k_p is the intraparticle diffusion rate constant ($\text{mg g}^{-1} \text{s}^{-0.5}$) and C is a constant for any experiment.

■ ASSOCIATED CONTENT

SI Supporting Information

The Supporting Information is available free of charge at <https://pubs.acs.org/doi/10.1021/acsomega.4c00037>.

XRD patterns of β -CD, cellulose, PVA, and β -CD/cellulose/PVA hydrogels (Figure S1); (a) XPS spectra of hydrogels, (b) XPS high-resolution C 1s spectra of the CP1C hydrogel before and after malathion adsorption, and (c) O 1s spectra of the CP1C hydrogel before and after malathion adsorption (Figure S2); N_2 adsorption-desorption isotherm of CP1C hydrogel (Figure S3); and

solid-state ^{13}C NMR spectra for (a) β -CD/cellulose/PVA hydrogels and (b) CP1C sample for before and after malathion adsorption (Figure S4) (PDF)

■ AUTHOR INFORMATION

Corresponding Author

Chalida Niamnuy – Department of Chemical Engineering, Faculty of Engineering, Kasetsart University, Bangkok 10900, Thailand; Research Network NANOTEC-Kasetsart on NanoCatalysts and NanoMaterials for Sustainable Energy and Environment: RNN-CMSEE and Center for Advanced Studies in Nanotechnology for Chemical, Food and Agricultural Industrials, Kasetsart University, Bangkok 10900, Thailand; orcid.org/0000-0003-2932-2022; Phone: +66 2 797 0999; Email: fengcdni@ku.ac.th; Fax: +66 2 561 4621

Authors

Maneerat Thongrueng – Department of Chemical Engineering, Faculty of Engineering, Kasetsart University, Bangkok 10900, Thailand

Kandis Sudsakorn – Department of Chemical Engineering, Faculty of Engineering, Kasetsart University, Bangkok 10900, Thailand

Manop Charoenchaitrakool – Department of Chemical Engineering, Faculty of Engineering, Kasetsart University, Bangkok 10900, Thailand; Research Network NANOTEC-Kasetsart on NanoCatalysts and NanoMaterials for Sustainable Energy and Environment: RNN-CMSEE and Center for Advanced Studies in Nanotechnology for Chemical, Food and Agricultural Industrials, Kasetsart University, Bangkok 10900, Thailand

Anusorn Seubsai – Department of Chemical Engineering, Faculty of Engineering, Kasetsart University, Bangkok 10900, Thailand; Research Network NANOTEC-Kasetsart on NanoCatalysts and NanoMaterials for Sustainable Energy and Environment: RNN-CMSEE and Center for Advanced Studies in Nanotechnology for Chemical, Food and Agricultural Industrials, Kasetsart University, Bangkok 10900, Thailand; orcid.org/0000-0001-8336-6590

Noppadol Panchan – Faculty of Engineering and Technology, Mahanakorn University of Technology, Bangkok 10530, Thailand

Sakamon Devahastin – Advanced Food Processing Research Laboratory, Department of Food Engineering, Faculty of Engineering, King Mongkut's University of Technology Thonburi, Bangkok 10140, Thailand; The Academy of Science, The Royal Society of Thailand, Bangkok 10300, Thailand

Complete contact information is available at:

<https://pubs.acs.org/10.1021/acsomega.4c00037>

Author Contributions

M.T.: Investigation, formal analysis, writing—original draft preparation, and visualization. K.S.: Reviewing and editing. Manop Charoenchaitrakool: Reviewing and editing. A.S.: Reviewing and editing. Noppadol Panchan: Reviewing and editing. S.D.: Conceptualization, funding acquisition, and writing—reviewing and editing. C.N.: Conceptualization, funding acquisition, supervision, investigation, and writing—reviewing and editing.

Notes

The authors declare no competing financial interest.

ACKNOWLEDGMENTS

This research was funded by Kasetsart University through the Graduate School Fellowship Program and the Fundamental Fund, Thailand (FF (KU) 12.66) and the Kasetsart University Research and Development Institute (KURDI), Bangkok, Thailand. The study was also supported by the National Science and Technology Development Agency (NSTDA) through the Chair Professor Grant (Grant No. P-20-52263). All authors express their sincere gratitude to Advanced Biochemical (Thailand) Co., Ltd. (Rayong, Thailand) for providing the biobased epichlorohydrin used in the experiments.

REFERENCES

- (1) Damalas, C. A.; Eleftherohorinos, I. G. Pesticide Exposure, Safety Issues, and Risk Assessment Indicators. *Int. J. Environ. Res. Public Health* **2011**, *8*, 1402–1419.
- (2) Arias-Estévez, M.; López-Periago, E.; Martínez-Carballo, E.; Simal-Gándara, J.; Mejuto, J. C.; García-Río, L. The mobility and degradation of pesticides in soils and the pollution of groundwater resources. *Agric., Ecosyst. Environ.* **2008**, *123*, 247–260.
- (3) Bodnar, O.; Horyn, O.; Khatib, I.; Falfushynska, H. Multi-biomarker assessment in zebrafish *Danio rerio* after the effects of malathion and chlorpyrifos. *Toxicol. Environ. Health Sci.* **2021**, *13*, 165–174.
- (4) Poomagal, S.; Sujatha, R.; Kumar, P. S.; Vo, D. N. A fuzzy cognitive map approach to predict the hazardous effects of malathion to environment (air, water and soil). *Chemosphere* **2021**, *263*, No. 127926.
- (5) Hosseini, M.; Kamani, H.; Esrafil, A.; Yegane Badi, M.; Gholami, M. Removal of Malathion by Sodium Alginate/Biosilicate/Magnetite Nanocomposite as a Novel Adsorbent: Kinetics, Isotherms, and Thermodynamic Study. *Health Scope* **2019**, *8*, No. e88454.
- (6) Jensen, I. M.; Whatling, P. Malathion: A Review of Toxicology. In *Hayes' Handbook of Pesticide Toxicology*, 3rd ed.; Krieger, R., Ed.; Academic Press: Cambridge, 2010; Chapter 71, pp 1527–1542.
- (7) Aris, N. I. F.; Rahman, N. A.; Wahid, M. H.; Yahaya, N.; Abdul Keyon, A. S.; Kamaruzaman, S. Superhydrophilic graphene oxide/electrospun cellulose nanofiber for efficient adsorption of organophosphorus pesticides from environmental samples. *R. Soc. Open Sci.* **2020**, *7*, No. 192050.
- (8) Habila, M. A.; AlOthman, Z. A.; Al-Tamrah, S. A.; Ghafar, A. A. Activated carbon from waste as an efficient adsorbent for malathion for detection and removal purposes. *J. Ind. Eng. Chem.* **2015**, *32*, 336–344.
- (9) Dehghani, M. H.; Niasar, Z. S.; Mehrnia, M. R.; Shayeghi, M.; Al-Ghouti, M. A.; Heibati, B.; McKay, G.; Yetilmezsoy, K. Optimizing the removal of organophosphorus pesticide malathion from water using multi-walled carbon nanotubes. *Chem. Eng. J.* **2017**, *310*, 22–32.
- (10) Gao, Y.; Gao, M.; Chen, G.; Tian, M.; Zhai, R.; Huang, X.; Xu, X.; Liu, G.; Xu, D. Facile synthesis of covalent organic frameworks functionalized with graphene hydrogel for effectively extracting organophosphorus pesticides from vegetables. *Food Chem.* **2021**, *352*, No. 129187.
- (11) Mondol, M. M. H.; Jhung, S. H. Adsorptive removal of pesticides from water with metal-organic framework-based materials. *Chem. Eng. J.* **2021**, *421*, No. 129688.
- (12) Kyriakopoulos, G. G.; Hourdakias, A.; Doulia, D. Adsorption of pesticides on resins. *J. Environ. Sci. Health, Part B* **2003**, *38*, 157–168.
- (13) Ahmad, T.; Rafatullah, M.; Ghazali, A.; Sulaiman, O.; Hashim, R.; Ahmad, A. Removal of pesticides from water and wastewater by different adsorbents: A review. *J. Environ. Sci. Health, Part C* **2010**, *28*, 231–271.
- (14) Kumar, P.; Singh, H.; Kapur, M.; Mondal, M. K. Comparative study of malathion removal from aqueous solution by agricultural and commercial adsorbents. *J. Water Process Eng.* **2014**, *3*, 67–73.
- (15) Abd El-Mohdy, H. L.; Hegazy, E. A.; El-Nesr, E. M.; El-Wahab, M. A. Removal of Some Pesticides from Aqueous Solutions using PVP/(AAc-co-Sty) Hydrogels Prepared by Gamma Radiation. *J. Macromol. Sci., Part A: Pure Appl. Chem.* **2012**, *49*, 814–827.
- (16) Sharma, P.; Laddha, H.; Agarwal, M.; Gupta, R. Selective and effective adsorption of malachite green and methylene blue on a non-toxic, biodegradable, and reusable fenugreek galactomannan gum coupled MnO₂ mesoporous hydrogel. *Microporous Mesoporous Mater.* **2022**, *338*, No. 111982.
- (17) Ho, T. C.; Chang, C. C.; Chan, H. P.; Chung, T. W.; Shu, C. W.; Chuang, K. P.; Duh, T. H.; Yang, M. H.; Tyan, Y. C. Hydrogels: Properties and Applications in Biomedicine. *Molecules* **2022**, *27*, 2902.
- (18) Sharma, P.; Sharma, M.; Laddha, H.; Gupta, R.; Agarwal, M. Non-toxic and biodegradable κ -carrageenan/ZnO hydrogel for adsorptive removal of norfloxacin: Optimization using response surface methodology. *Int. J. Biol. Macromol.* **2023**, *238*, No. 124145.
- (19) Bind, A.; Tiwari, A. Synthesis and characterization of paramagnetic (poly styrene-coacrylamide) hydrogel: use as adsorbent for removal of pesticide (chlorpyrifos). *IOSR J. Environ. Sci., Toxicol. Food Technol.* **2016**, *10*, 108–113.
- (20) Hassanzadeh-Afruzi, F.; Maleki, A.; Maleki, A.; Zare, E. N. Efficient remediation of chlorpyrifos pesticide from contaminated water by superparamagnetic adsorbent based on Arabic gum-grafted-poly-amidoxime. *Int. J. Biol. Macromol.* **2022**, *203*, 1445–456.
- (21) Li, Y.; Xu, X.; Guo, H.; Bian, Y.; Li, J.; Zhang, F. Magnetic graphene oxide-based covalent organic frameworks as novel adsorbent for extraction and separation of triazine herbicides from fruit and vegetable samples. *Anal. Chim. Acta* **2022**, *1219*, No. 339984.
- (22) Xing, C. Y.; Zeng, S. L.; Qi, S. K.; Jiang, M. J.; Xu, L.; Chen, L.; Zhang, S.; Li, B. J. Poly(vinyl alcohol)/ β -cyclodextrin composite fiber with good flame retardant and super-smoke suppression properties. *Polymers* **2020**, *12*, 1078.
- (23) Chang, C.; Lue, A.; Zhang, L. Effects of Crosslinking Methods on Structure and Properties of Cellulose/PVA Hydrogels. *Macromol. Chem. Phys.* **2008**, *209*, 1266–1273.
- (24) Ban, M. T.; Mahadin, N.; Abd Karim, K. J. Synthesis of hydrogel from sugarcane bagasse extracted cellulose for swelling properties study. *Mater. Today: Proc.* **2022**, *50*, 2567–2575.
- (25) Zhang, L.; Zhou, J.; Zhang, L. Structure and properties of beta-cyclodextrin/cellulose hydrogels prepared in NaOH/urea aqueous solution. *Carbohydr. Polym.* **2013**, *94*, 386–393.
- (26) Sharma, P.; Sharma, M.; Laddha, H.; Agarwal, M.; Gupta, R. Effective adsorption–desorption kinetic study and statistical modeling of bentazon herbicide mediated by a biodegradable β -cyclodextrin cross-linked poly(vinyl alcohol)–chitosan hydrogel. *ACS Agric. Sci. Technol.* **2023**, *3*, 1068–1080.
- (27) Tapia, M. S.; Alzamora, S. M.; Chirife, J. Effects of Water Activity (a_w) on Microbial Stability as a Hurdle in Food Preservation. In *Water Activity in Foods: Fundamentals and Applications*; Barbosa-Cánovas, G. V.; Fontana, A. J., Jr.; Schmidt, S. J.; Labuza, T. P., Eds.; John Wiley & Sons, Inc: New York, 2020; pp 323–355.
- (28) Kundu, D.; Mondal, S. K.; Banerjee, T. Development of β -Cyclodextrin-Cellulose/Hemicellulose-Based Hydrogels for the Removal of Cd(II) and Ni(II): Synthesis, Kinetics, and Adsorption Aspects. *J. Chem. Eng. Data* **2019**, *64*, 2601–2617.
- (29) Wang, L.-Y.; Wang, M.-J. Removal of Heavy Metal Ions by Poly(vinyl alcohol) and Carboxymethyl Cellulose Composite Hydrogels Prepared by a Freeze–Thaw Method. *ACS Sustainable Chem. Eng.* **2016**, *4*, 2830–2837.
- (30) Sankarganesh, P.; Parthasarathy, V.; Ganesh Kumar, A.; Ragu, S.; Saraniya, M.; Udayakumari, N.; Anbarasan, R. Preparation of Cellulose-PVA Blended Hydrogels for Wound Healing Applications with Controlled Release of the Antibacterial Drug: An In Vitro Anticancer Activity. In *Biomass Conversion and Biorefinery*; Springer, 2022.

- (31) Hemine, K.; Lukasik, N.; Gazda, M.; Nowak, I. β -cyclodextrin-containing polymer based on renewable cellulose resources for effective removal of ionic and non-ionic toxic organic pollutants from water. *J. Hazard. Mater.* **2021**, *418*, No. 126286.
- (32) Quintás, G.; Morales-Noé, A.; Armenta, S.; Garrigues, S.; de la Guardia, M. Fourier transform infrared spectrometric determination of Malathion in pesticide formulations. *Anal. Chim. Acta* **2004**, *502*, 213–220.
- (33) Vinayan, B. P.; Zhao-Karger, Z.; Diemant, T.; Chakravadhanula, V. S.; Schwarzburger, N. I.; Cambaz, M. A.; Behm, R. J.; Kubel, C.; Fichtner, M. Performance study of magnesium-sulfur battery using a graphene based sulfur composite cathode electrode and a non-nucleophilic Mg electrolyte. *Nanoscale* **2016**, *8*, 3296–3306.
- (34) Naushad, M.; Allothman, Z. A.; Khan, M. R. Removal of malathion from aqueous solution using De-Acidite FF-IP resin and determination by UPLC-MS/MS: equilibrium, kinetics and thermodynamics studies. *Talanta* **2013**, *115*, 15–23.
- (35) Letort, S.; Balieu, S.; Erb, W.; Gouhier, G.; Estour, F. Interactions of cyclodextrin and their derivatives with toxic organophosphorus compounds. *Beilstein J. Org. Chem.* **2016**, *12*, 204–228.
- (36) Peng, H.; Wang, S.; Xu, H.; Hao, X. Preparation, properties and formation mechanism of cellulose/polyvinyl alcohol bio-composite hydrogel membranes. *New J. Chem.* **2017**, *41*, 6564–6573.
- (37) Zhang, Z.; Li, Q.; Yesildang, C.; Bartsch, C.; Zhang, X.; Liu, W.; Loebus, A.; Su, Z.; Lensen, M. C. Influence of network structure on the crystallization behavior in chemically crosslinked hydrogels. *Polymers* **2018**, *10*, 970.
- (38) Yang, H.; Xu, S.; Jiang, L.; Dan, Y. Thermal Decomposition Behavior of Poly (Vinyl Alcohol) with Different Hydroxyl Content. *J. Macromol. Sci., Part B: Phys.* **2012**, *51*, 464–480.
- (39) Nada, A. M. A.; Yousef, H. A.; El-Gohary, S. Thermal degradation of hydrolyzed and oxidized lignins. *J. Therm. Anal. Calorim.* **2002**, *68*, 265–273.
- (40) Jayaramudu, T.; Ko, H.-U.; Zhai, L.; Li, Y.; Kim, J. Preparation and Characterization of Hydrogels from Polyvinyl alcohol and Cellulose and their Electroactive behavior. *Soft Matter* **2017**, *15*, 64–72.
- (41) Wang, H.; Li, J.; Ding, N.; Zeng, X.; Tang, X.; Sun, Y.; Lei, T.; Lin, L. Eco-friendly polymer nanocomposite hydrogel enhanced by cellulose nanocrystal and graphitic-like carbon nitride nanosheet. *Chem. Eng. J.* **2020**, *386*, No. 124021.
- (42) Wang, Y.; Liu, S.; Wang, Q.; Fu, X.; Fatehi, P. Performance of polyvinyl alcohol hydrogel reinforced with lignin-containing cellulose nanocrystals. *Cellulose* **2020**, *27*, 8725–8743.
- (43) Zhang, R.; Zhou, Z.; Xie, A.; Dai, J.; Cui, J.; Lang, J.; Wei, M.; Dai, X.; Li, C.; Yan, Y. Preparation of hierarchical porous carbons from sodium carboxymethyl cellulose via halloysite template strategy coupled with KOH-activation for efficient removal of chloramphenicol. *J. Taiwan Inst. Chem. Eng.* **2017**, *80*, 424–433.
- (44) Martwong, E.; Sukhawipat, N.; Junthip, J. Cotton Cord Coated with Cyclodextrin Polymers for Paraquat Removal from Water. *Polymers* **2022**, *14*, 2199.
- (45) Mjakin, S. V.; Sychov, M. M.; Sheiko, N. B.; Ezhenkova, L. L.; Rodionov, A. G.; Vasiljeva, I. V. Improvement of vibrodamping properties of polyvinyl acetate-graphite composites by electron beam processing of the filler. *SpringerPlus* **2016**, *5*, 1539.
- (46) Roata, I. C.; Croitoru, C.; Pascu, A.; Stanciu, E. M. Characterization of physically crosslinked ionic liquid-lignocellulose hydrogels. *BioResources* **2018**, *13*, 6110–6121.
- (47) Thommes, M.; Kaneko, K.; Neimark, A. V.; Olivier, J. P.; Rodriguez-Reinoso, F.; Rouquerol, J.; Sing, K. S. W. Physisorption of gases, with special reference to the evaluation of surface area and pore size distribution (IUPAC Technical Report). *Pure Appl. Chem.* **2015**, *87*, 1051–1069.
- (48) Sergeeva, A.; Vikulina, A. S.; Volodkin, D. Porous alginate scaffolds assembled using vaterite CaCO₃ crystals. *Micromachines* **2019**, *10*, 357.
- (49) Adjuik, T. A.; Nokes, S. E.; Montross, M. D. Biodegradability of bio-based and synthetic hydrogels as sustainable soil amendments: A review. *J. Appl. Polym. Sci.* **2023**, *140*, No. e53655.
- (50) Panchan, N.; Niannuy, C.; Dittanet, P.; Devahastin, S. Optimization of synthesis condition for carboxymethyl cellulose-based hydrogel from rice straw by microwave-assisted method and its application in heavy metal ions removal. *J. Chem. Technol. Biotechnol.* **2018**, *93*, 413–425.
- (51) Naushad, M.; Allothman, Z. A.; Khan, M. R.; Alqahtani, N. J.; Alsoghaimi, I. H. Equilibrium, kinetics and thermodynamic studies for the removal of organophosphorus pesticide using Amberlyst-15 resin: Quantitative analysis by liquid chromatography–mass spectrometry. *J. Ind. Eng. Chem.* **2014**, *20*, 4393–4400.
- (52) Gangadhar, B.; Yadamari, T.; Korivi, S. K.; Gurijala, R. N.; Singhal, R. K. Study on degradation of malathion and phorate in various environmental matrices. *Afr. J. Environ. Sci. Technol.* **2012**, *6*, 224–228.
- (53) Abdeen, Z.; Mohammad, S. G. Study of the Adsorption Efficiency of an Eco-Friendly Carbohydrate Polymer for Contaminated Aqueous Solution by Organophosphorus Pesticide. *Open J. Org. Polym. Mater.* **2014**, *04*, 16–28.
- (54) Azady, M. A. R.; Alam, M. S.; Paul, S. C.; Rahaman, M. S.; Sultana, S.; Hasnine, S. M. M.; Ahmed, T.; Gafur, M. A. Preparation and Characterization of Gamma Radiation Assisted Poly-Vinyl Alcohol/Acrylic Acid/Poly-4-Styrene Sulphonic Acid Based Hydrogel: Application for Textile Dye Removal. *J. Polym. Environ.* **2021**, *29*, 520–537.
- (55) Ishtiaq, F.; Bhatti, H. N.; Khan, A.; Iqbal, M.; Kausar, A. Polypyrrole, polyaniline and sodium alginate biocomposites and adsorption-desorption efficiency for imidacloprid insecticide. *Int. J. Biol. Macromol.* **2020**, *147*, 217–232.
- (56) Vegas-Mendoza, S. M.; Gutierrez-Ortega, J. A.; Moran-Salazar, R. G.; Cortes-Llamas, S. A.; Carbajal-Arizaga, G. G.; Peregrina-Lucano, A. A.; Shenderovich, I. G.; Torres-Santiago, G.; Gómez-Salazar, S. L-Glutathione-Functionalized Silica Adsorbent for the Removal of Pesticide Malathion from Aqueous Solutions. *Processes* **2022**, *10*, 2146.
- (57) Singh, V. K.; Singh, R. S.; Tiwari, P. N.; Singh, J. K.; Gode, F.; Sharma, Y. C. Removal of Malathion from Aqueous Solutions and Waste Water Using Fly Ash. *J. Water Resour. Prot.* **2010**, *02*, 322–330.
- (58) Kalantary, R. R.; Azari, A.; Esrafil, A.; Yaghmaeian, K.; Moradi, M.; Sharafi, K. The survey of Malathion removal using magnetic graphene oxide nanocomposite as a novel adsorbent: thermodynamics, isotherms, and kinetic study. *Desalin. Water Treat.* **2016**, *57*, 28460–28473.
- (59) Sabbagh, N.; Tahvildari, K.; Mehrdad Sharif, A. A. Application of chitosan-alginate bio composite for adsorption of malathion from wastewater: Characterization and response surface methodology. *J. Contam. Hydrol.* **2021**, *242*, No. 103868.
- (60) Sabbagh, N.; Tahvildari, K.; Mehrdad Sharif, A. A. Highly efficient and rapid removal of malathion using crosslinked chitosan-alginate nanocomposites and optimization of parameters by box-behnken design: isotherms and kinetic studies. *J. Polym. Environ.* **2023**, *31*, 2595–2611.
- (61) AOAC. *Official Methods of Analysis of AOAC International*, 17th ed.; AOAC International: MD, 2000.
- (62) Hajiabbas, M.; Alemzadeh, I.; Vossoughi, M. A porous hydrogel-electrospun composite scaffold made of oxidized alginate/gelatin/silk fibroin for tissue engineering application. *Carbohydr. Polym.* **2020**, *245*, No. 116465.
- (63) Nigam, S.; Das, A. K.; Patidar, M. K. Synthesis, characterization and biodegradation of Bioplastic films produced from Parthenium hysterophorus by incorporating a plasticizer (PEG600). *Environ. Challenges* **2021**, *5*, No. 100280.
- (64) Prasath, R. R.; Muthirulan, P.; Kannan, N. Agricultural wastes as a low cost adsorbents for the removal of Acid Blue 92 dye: A comparative study with commercial activated carbon. *IOSR J. Agric. Vet. Sci.* **2014**, *7*, 19–32.

- (65) Obaid, S. A. Langmuir, Freundlich and Tamkin Adsorption Isotherms and Kinetics for The Removal Aartichoke Tournefortii Straw from Agricultural Waste. *J. Phys. Conf. Ser.* **2020**, *1664*, No. 012011.
- (66) Ebelegi, A. N.; Ayawei, N.; Wankasi, D. Interpretation of Adsorption Thermodynamics and Kinetics. *Open J. Phys. Chem.* **2020**, *10*, 166–182.
- (67) Wu, F.-C.; Tseng, R.-L.; Juang, R.-S. Initial behavior of intraparticle diffusion model used in the description of adsorption kinetics. *Chem. Eng. J.* **2009**, *153*, 1–8.